Global-Position Tracking Control of a Fully Actuated NAO Bipedal Walking Robot

Yuan Gao and Yan Gu

Abstract— **The ability to reliably track various planned paths with specific timing, which is termed as the global-position tracking capability in this paper, is essential to highly versatile bipedal robotic walking. To provably guarantee global-position tracking performance for fully actuated bipedal robots, this study proposes a time-dependent state-feedback control strategy based on a) a full-order model of the hybrid, nonlinear, floating-based bipedal walking dynamics, b) time-dependent input-output linearization, and c) Lyapunov-based stability analysis. This study also provides general guidelines for adapting the proposed control strategy to walking experiments in the presence of a common hardware limitation of bipedal robots, which will help to bridge the gap between theory and experiment in bipedal walking control. Simulations and experiments on a NAO bipedal robot were performed to demonstrate the effectiveness of the proposed walking control strategy.**

I. INTRODUCTION

Versatility of bipedal robotic walking refers to a robot's ability to purposefully perform different motions [1]. An important aspect of enabling versatile walking is to realize reliable tracking of various planned trajectories of a robot's global position (i.e., a robot's based position in the world coordinate frame). Global-position tracking control has been extensively investigated and successfully implemented on various bipedal robots through the Zero-Moment-Point (ZMP) approach [2]–[4]. Despite the high versatility, the ZMP approach can only realize relatively low agility and energy efficiency and cannot provably guarantee the stability of the closed-loop walking control system [5], [6].

To produce provably stable, agile, and efficient walking, the Hybrid-Zero-Dynamics (HZD) approach has been introduced based on full-order dynamic modeling, input-output linearizing state feedback control, and orbital stabilization [5], [7]. The HZD framework has realized agile bipedal gait for fully actuated [8], underactuated [9], [10], and multi-domain walking [11], as well as running [12] and robot-assisted human walking [13]. Recently, velocity regulation [4] and learning-based gait library design [14] have been incorporated into the HZD framework to enhance walking versatility beyond periodic walking.

Inspired by the HZD approach, we have introduced time-dependent feedback control to achieve exponential global-position tracking for enhancing walking versatility of fully actuated planar bipedal robots [15], [16]. To our best knowledge, it is the first time that exponential global-position tracking has been provably produced for bipedal robotic walking. This control strategy has been theoretically extended to a 3-D bipedal robot with 9 DOFs and validated through simulations [17].

In this study, our previous global-position tracking control will be further extended to a general three-dimensional (3-D) bipedal robot model and experimentally evaluated on a NAO bipedal humanoid robot [18]. This paper has two main contributions. The first main contribution is a set of formally constructed sufficient conditions that provably guarantee the exponential global-position tracking performance of the proposed control strategy. The second main contribution is experimental guidelines that can be used to adapt the proposed global-position tracking controller to a representative bipedal robot platform with a common control implementation limitation, which will help to bridge the gap between theory and experiment in bipedal walking control.

This paper is organized as follows. Section II presents the hybrid full-order model of bipedal walking dynamics. The proposed global-position tracking control is explained in Section III, including the derivation of trajectory tracking errors, the construction of impact invariance conditions, and the analysis of closed-loop system stability. Section IV introduces simulation results for control design validation and hardware implementation preparation. Details of experimental validation are given in Section V, including general guidelines of controller adaptation for addressing a common hardware limitation of bipedal robots.

II. HYBRID FLOATING-BASED DYNAMICS OF BIPEDAL ROBOTIC WALKING

This section presents a full-order model of bipedal walking dynamics, which provides a faithful description of the hybrid, nonlinear dynamic behaviors of all degrees of freedom involved in walking and will be utilized in the design of the proposed model-based feedback control in Section III.

Because bipedal robotic walking is inherently hybrid involving both continuous dynamics (e.g., foot swinging) and discrete behaviors (e.g., foot landings), it is natural to model a bipedal walking process as a hybrid dynamical system. The following modeling assumptions are considered in this study: a) The walking surface is even and horizontal; b) During a single-support phase, the robot's support foot remains full, static contact with the walking surface; c) The landing event is modeled as an impact between rigid bodies, and a double-support phase is instantaneous [5].

The generalized coordinates of a floating-based bipedal robot can be denoted as

Yuan Gao and Yan Gu are with the Department of Mechanical Engineering, University of Massachusetts Lowell, Lowell, MA 01854, U.S.A. Emails: yuan_gao@student.uml.edu, yan_gu@uml.edu.

$$\mathbf{q} = \left[\mathbf{p}_b^T, \boldsymbol{\gamma}_b^T, q_1, ..., q_n\right]^T \in \mathcal{Q}, \tag{1}$$

where $\mathcal{Q} \subset \mathbb{R}^{n+6}$ is the configuration space, $\mathbf{p}_b := [x_b, y_b, z_b]^T \in \mathbb{R}^3$ represents the floating-base position with respect to (w.r.t.) the world coordinate frame, which is used to represent the robot's global position in this study, $\boldsymbol{\gamma}_b := [\phi_b, \theta_b, \psi_b]^T$ represents the vector of pitch, roll, and yaw angles of the floating base w.r.t. the world coordinate frame, and $q_1, ..., q_n$ represent the robot's joint angles.

The NAO robot (Fig. 1) has 24 joints (i.e., $n = 24$). Due to the mechanical coupling between the two hip joints and the holonomic constraint that the support foot remains static, full contact with the walking surface, the robot has 23 DOFs. Since it also has 23 independent joint actuators, the robot is fully actuated.

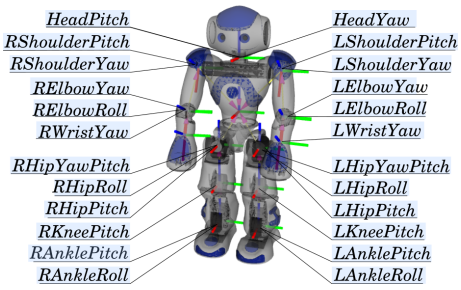

Fig. 1. An illustration of the revolute joints of a NAO bipedal humanoid robot. The coordinate system of the robot's floating base is located at the center of the chest.

A. Continuous-Phase Dynamics

With Lagrange's method, bipedal walking dynamics during a continuous phase can be obtained as [5]:

$$\mathbf{M}(\mathbf{q})\ddot{\mathbf{q}} + \mathbf{c}(\mathbf{q}, \dot{\mathbf{q}}) = \mathbf{B}\mathbf{u} + \mathbf{J}^T\mathbf{F}, \tag{2}$$

where $\mathbf{M}(\mathbf{q}) : \mathcal{Q} \to \mathbb{R}^{(n+6)\times(n+6)}$ is the inertia matrix, $\mathbf{c}(\mathbf{q}, \dot{\mathbf{q}}) : \mathcal{TQ} \to \mathbb{R}^{(n+6)\times(n+6)}$ is the sum of Coriolis, centrifugal, and gravitational terms, $\mathbf{B} \in \mathbb{R}^{(n+6)\times m}$ ($m = 23$) is a constant matrix, and $\mathbf{u} \in \mathbb{R}^m$ is the joint torque vector. Here, $\mathbf{F} \in \mathbb{R}^7$ is the vector of the ground-reaction force applied at the support foot and the internal force between the two mechanically coupled hip joints, and $\mathbf{J}$ is the associated Jacobian matrix. The holonomic constraints that the NAO robot is subject to can be described as [19]:

$$\mathbf{J}\ddot{\mathbf{q}} + \dot{\mathbf{J}}\dot{\mathbf{q}} = \mathbf{0}. \tag{3}$$

From Eqs. (2) and (3), the continuous-phase dynamics can be compactly expressed as:

$$\mathbf{M}(\mathbf{q})\ddot{\mathbf{q}} + \bar{\mathbf{c}}(\mathbf{q}, \dot{\mathbf{q}}) = \bar{\mathbf{B}}(\mathbf{q})\mathbf{u}, \tag{4}$$

where the derivations of $\bar{\mathbf{c}}(\mathbf{q}, \dot{\mathbf{q}})$ and $\bar{\mathbf{B}}(\mathbf{q})$ are shown next.

From Eq. (2), one has

$$\ddot{\mathbf{q}} = \mathbf{M}^{-1}(-\mathbf{c} + \mathbf{B}\mathbf{u} + \mathbf{J}^T\mathbf{F}). \tag{5}$$

Substituting Eq. (5) into Eqs. (3) yields:

$$\mathbf{F} = (\mathbf{J}\mathbf{M}^{-1}\mathbf{J}^{\mathbf{T}})^{-1}(\mathbf{J}\mathbf{M}^{-1}\mathbf{c} - \dot{\mathbf{J}}\dot{\mathbf{q}} - \mathbf{J}\mathbf{M}^{-1}\mathbf{B}\mathbf{u}). \tag{6}$$

Substituting Eq. (6) into Eq. (2), the expressions of $\bar{\mathbf{c}}(\mathbf{q}, \dot{\mathbf{q}})$ and $\bar{\mathbf{B}}(\mathbf{q})$ can be obtained as:

$$\begin{aligned} \bar{\mathbf{c}}(\mathbf{q}, \dot{\mathbf{q}}) &= \mathbf{c} - \mathbf{J}^{\mathbf{T}}(\mathbf{J}\mathbf{M}^{-1}\mathbf{J}^{\mathbf{T}})^{-1}(\mathbf{J}\mathbf{M}^{-1}\mathbf{c} - \dot{\mathbf{J}}\dot{\mathbf{q}}); \\ \bar{\mathbf{B}}(\mathbf{q}) &= \mathbf{B} - \mathbf{J}^{\mathbf{T}}(\mathbf{J}\mathbf{M}^{-1}\mathbf{J}^{\mathbf{T}})^{-1}\mathbf{J}\mathbf{M}^{-1}\mathbf{B}. \end{aligned} \tag{7}$$

B. Switching Surface

A switching event that connects a continuous single-support phase with a subsequent instantaneous double-support phase can be described by a switching surface:

$$S_q(\mathbf{q}, \dot{\mathbf{q}}) := \{(\mathbf{q}, \dot{\mathbf{q}}) \in \mathcal{TQ} : z_{sw}(\mathbf{q}) = 0, \dot{z}_{sw}(\mathbf{q}, \dot{\mathbf{q}}) < 0\}, \tag{8}$$

where $z_{sw} : \mathcal{Q} \to \mathbb{R}$ represents the swing-foot height above the walking surface.

C. Reset Map

When the swing foot hits the walking surface, an instantaneous rigid-body impact occurs. The robot's joint positions will remain continuous upon the impact. But the joint velocities will experience a sudden jump, which can be described by the following reset map:

$$\dot{\mathbf{q}}^+ = \mathbf{R}_{\dot{\mathbf{q}}}(\mathbf{q}^-)\dot{\mathbf{q}}^-, \tag{9}$$

where $\dot{\mathbf{q}}^-$ and $\dot{\mathbf{q}}^+$ denote the values of $\dot{\mathbf{q}}$ right before and after an impact. Here, $\mathbf{R}_{\dot{q}} : \mathcal{Q} \to \mathbb{R}^{(n+6)\times(n+6)}$ can be obtained by solving

$$\begin{bmatrix} \mathbf{M}(\mathbf{q}^-) & -\mathbf{J}^T(\mathbf{q}^-) \\ \mathbf{J}^T(\mathbf{q}^-) & \mathbf{0}_{7\times7} \end{bmatrix} \begin{bmatrix} \dot{\mathbf{q}}^+ \\ \delta\mathbf{F} \end{bmatrix} = \begin{bmatrix} \mathbf{M}(\mathbf{q}^-)\dot{\mathbf{q}}^- \\ \mathbf{0}_{7\times1} \end{bmatrix},$$

where $\delta\mathbf{F}$ is a vector of the impulsive ground-reaction force and hip coupling force, and $\mathbf{0}_{7\times7}$ is a 7×7 zero matrix.

III. Time-Dependent Global-Position Tracking Control

The primary control objective of this study is to achieve satisfactory tracking of the desired global-position trajectory along the desired global path on the walking surface for a fully actuated NAO bipedal walking robot. To realize this objective, a time-dependent, model-based feedback controller is synthesized based on the dynamic model presented in Section II, input-output linearization, and Lyapunov-based stability analysis.

A. Trajectory Tracking Errors

Let $\mathbf{h}_c(\mathbf{q}) : Q \to Q_c \subset \mathbb{R}^m$ denote the variables of interest to be controlled, which include: a) the robot's global position, represented by the floating-base position, (x_b, y_b, z_b); b) the floating-base roll angle, ϕ_b, and pitch angle, θ_b; c) the swing-foot position and orientation, denoted as $\mathbf{p}_{sw}(\mathbf{q}) \in \mathbb{R}^3$ and $\boldsymbol{\gamma}_{sw}(\mathbf{q}) \in \mathbb{R}^3$, respectively; d) the upper-body joint angles, $\mathbf{q}_{upper} \in \mathbb{R}^{n_{upper}}$ ($n_{upper} = 12$ for the NAO robot in Fig. 1). Accordingly, $\mathbf{h}_\mathbf{c}(\mathbf{q})$ is defined as:

$$\mathbf{h}_c(\mathbf{q}) := \left[x_b, y_b, z_b, \phi_b, \theta_b, \mathbf{p}_{sw}^T(\mathbf{q}), \gamma_{sw}^T(\mathbf{q}), \mathbf{q}_{upper}^T\right]^T.$$

Let $\mathbf{h}_d(t, \theta(\mathbf{q})) : \mathbb{R}^+ \times \mathbb{R} \to \mathbb{R}^m$ denote the desired position trajectories of $\mathbf{h}_c(\mathbf{q})$, which are encoded by time t and a configuration-based variable $\theta : \mathcal{Q} \to \mathbb{R}$ that increases

monotonically within a step and represents how far a step has progressed. The desired global path on the walking surface, denoted as Γ_d, is chosen as a straight-line path in this study. For simplicity and without loss of generality, Γ_d is specified as the X_W-axis of the world coordinate frame $\Sigma_{X_W Y_W Z_W}$, i.e., $\Gamma_d := \{(X_W, Y_W) \in \mathbb{R}^2 : Y_W = 0\}$. The desired position trajectory along Γ_d is denoted as $x_d(t)$, which is an explicit function of time t. In previous work under the HZD framework [20], the desired trajectories are typically designed as state-based alone instead of time-dependent. Here, we define the desired global-position trajectory as explicitly time-dependent because desired global-position trajectories are often expressed as time functions in practical robotic applications.

With Γ_d and $x_d(t)$ defined, the desired trajectory $\mathbf{h}_d(t, \theta(\mathbf{q}))$ is defined as

$$\mathbf{h}_d(t, \theta(\mathbf{q})) := [x_d(t), \boldsymbol{\phi}^T(\theta(\mathbf{q}))]^T, \tag{10}$$

where $\boldsymbol{\phi}(\theta) : \mathbb{R} \to \mathbb{R}^{m-1}$ represents the desired trajectories of y_b, z_b, ϕ_b, θ_b, $\mathbf{p}_{sw}$, and $\boldsymbol{\gamma}_{sw}$. We can use Bézier polynomials to parameterize the desired function $\boldsymbol{\phi}(\theta)$ as [20]

$$\boldsymbol{\phi}(s) := \sum_{k=0}^{M} \boldsymbol{\alpha}_k \frac{M!}{k!(M-k)!} s^k (1-s)^{M-k}, \tag{11}$$

where $s := \frac{\theta - \theta^+}{\theta^- - \theta^+}$ is the normalized θ, $\boldsymbol{\alpha}_k \in \mathbb{R}^{m-1}$ ($k = 0, 1, ..., M$) is a coefficient vector to be optimized in Section IV, θ^- and θ^+ denote the values of θ right before and after an impact associated with the desired gait, and M is the order of the Bézier polynomials.

As the control objectives of this study is to track the desired position trajectory $x_d(t)$ while following the desired path Γ_d, the desired trajectory of y_b (i.e., the first element of $\boldsymbol{\phi}(\theta)$) will be planned as a trajectory that varies around zero within a small bound. This desired trajectory design has three advantages as compared with our previous study [17] that focuses on driving y_b strictly to zero: a) The holonomic constraint that requires a secured foot-ground contact can be more easily met in motion planning, thus reducing the computational load of planning; b) The resulting gait will be more natural-looking; c) The robot will still be considered as following a straight-line path by tracking a small-magnitude sine-wave path about the straight line.

With the trajectory tracking errors compactly expressed as

$$\mathbf{h}(t, \mathbf{q}) := \mathbf{h}_c(\mathbf{q}) - \mathbf{h}_d(t, \theta(\mathbf{q})), \tag{12}$$

the control objective of this study becomes to drive $\mathbf{h}$ exponentially to zero.

B. Impact Invariance Condition

Since bipedal walking is a hybrid dynamical process, the desired trajectories $\mathbf{h}_d(t, \mathbf{q})$ should respect the reset map in Eq. (9). To meet this requirement, a set of time-dependent impact invariance conditions can be derived based on previous state-based impact invariance construction [20].

Let T_K ($K \in \mathbb{Z}^+$) denote the K^{th} actual impact moment, and let T_0 denote the initial moment of a walking process. Let τ_K denote the K^{th} desired impact moment assuming $\mathbf{y} = \mathbf{0}$ and $\dot{\mathbf{y}} = \mathbf{0}$ for all $t > T_{K-1}$. The time-dependent impact invariance conditions can be mathematically expressed as [17]:

$$\begin{aligned} &\mathbf{h}_c(\mathbf{q}(\tau_K^+)) = \mathbf{h}_d(\tau_K^+, \mathbf{q}(\tau_K^+)); \\ &\dot{\mathbf{h}}_c(\mathbf{q}(\tau_K^+), \mathbf{R}_{\dot{q}}(\mathbf{q}(\tau_K^-))\dot{\mathbf{q}}(\tau_K^-)) = \dot{\mathbf{h}}_d(\tau_K^+, \mathbf{q}(\tau_K^+), \mathbf{R}_{\dot{q}}(\mathbf{q}(\tau_K^-)\dot{\mathbf{q}}(\tau_K^-))), \end{aligned} \tag{13}$$

where τ_K^- and τ_K^+ denote the moments right before and after τ_K, respectively.

C. Model-based State Feedback Control

To simplify the nonlinear continuous-phase dynamics of bipedal robotic walking, input-output linearization is utilized to synthesize a feedback controller that realizes exponential tracking of the desired trajectories.

The output functions are defined as the trajectory tracking errors:

$$\mathbf{y} = \mathbf{h}(t, \mathbf{q}). \tag{14}$$

With the following input-output linearizing control law [21]

$$\mathbf{u} = (\frac{\partial \mathbf{h}}{\partial \mathbf{q}} \mathbf{M}^{-1} \bar{\mathbf{B}})^{-1} [(\frac{\partial \mathbf{h}}{\partial \mathbf{q}}) \mathbf{M}^{-1} \bar{\mathbf{c}} + \mathbf{v} - \frac{\partial^2 \mathbf{h}}{\partial t^2} - \frac{\partial}{\partial \mathbf{q}} (\frac{\partial \mathbf{h}}{\partial \mathbf{q}} \dot{\mathbf{q}}) \dot{\mathbf{q}}], \tag{15}$$

the continuous-phase dynamics in Eq. (4) become $\ddot{\mathbf{y}} = \mathbf{v}$. By choosing

$$\mathbf{v} = -\mathbf{K}_p \mathbf{y} - \mathbf{K}_d \dot{\mathbf{y}},$$

where $\mathbf{K}_p \in \mathbb{R}^{m \times m}$ and $\mathbf{K}_d \in \mathbb{R}^{m \times m}$ are positive definite diagonal matrices, one has $\ddot{\mathbf{y}} = -\mathbf{K}_d \dot{\mathbf{y}} - \mathbf{K}_p \mathbf{y}$.

Although the proposed control law in Eq. (15) can stabilize the continuous-phase dynamics with properly chosen $\mathbf{K}_p$ and $\mathbf{K}_d$, the reset map in Eq. (9) remains uncontrolled. Thus, the closed-loop stability will be formally analyzed next.

D. Closed-Loop Stability Analysis

The stability analysis of the hybrid, nonlinear, time-varying closed-loop system will be discussed as an extension of our previous work [17] in this subsection.

From the dynamic model presented in Section II and the proposed control law in Eq. (15), the closed-loop dynamics can be compactly written as:

$$\begin{cases} \dot{\mathbf{x}} = \mathbf{A}\mathbf{x} := \begin{bmatrix} \mathbf{0}_{m \times m} & \mathbf{I}_{m \times m} \\ -\mathbf{K}_p & -\mathbf{K}_d \end{bmatrix} \mathbf{x} & \text{if } (t, \mathbf{x}^-) \notin S(t, \mathbf{x}); \\ \mathbf{x}^+ = \Delta(t, \mathbf{x}^-) & \text{if } (t, \mathbf{x}^-) \in S(t, \mathbf{x}), \end{cases} \tag{16}$$

where $\mathbf{x} := \begin{bmatrix} \mathbf{y}^T, & \dot{\mathbf{y}}^T \end{bmatrix}^T \in \mathcal{X} \subset \mathbb{R}^{2m}$, $\mathbf{0}_{m \times m}$ and $\mathbf{I}_{m \times m}$ are $m \times m$ zero and identity matrices, respectively, and the expressions of $S : \mathbb{R}^+ \times \mathcal{X} \to \mathbb{R}^{2m-1}$ and $\Delta : \mathbb{R}^+ \times \mathcal{X} \to \mathcal{X}$ can be readily obtained from Eqs. (8), (9), and (14). Note that the reset map and the switching surface are both explicitly time-dependent due to the explicit time dependence of $\mathbf{y}$.

For notational simplicity, $\star(T_{k-1}^-) := \star|_{k-1}^-$ and $\star(T_{k-1}^+) := \star|_{k-1}^+$ will be used in the following stability analysis. Due to space limitations, a sketch of the analysis will be presented.

According to Lyapunov-based stability analysis of hybrid systems [22], the hybrid time-varying system in Eq. (16) is locally exponentially stable if there exists a Lyapunov

function candidate $V(\mathbf{x})$ and a positive number r such that for any $\mathbf{x}(T_0) \in B_r(\mathbf{0}) := \{\mathbf{x} \in \mathcal{X} : \|\mathbf{x}\| \leq r\}$:

(A) $V(\mathbf{x})$ exponentially decreases during each continuous phase;
(B) $\{V|_1^+, V|_2^+, V|_3^+ ...\}$ is a strictly decreasing sequence.

The condition (A) can be met by properly selecting the control gains $\mathbf{K}_p$ and $\mathbf{K}_d$ in Eq. (16). Specifically, if the control gains are chosen such that the matrix $\mathbf{A}$ in Eq. (16) is Hurwitz, then there exists a Lyapunov function candidate $V(\mathbf{x})$ and positive numbers c_1, c_2, and c_3 such that

$$c_1||\mathbf{x}||^2 \leq V(\mathbf{x}) \leq c_2||\mathbf{x}||^2$$

and

$$\dot{V}(\mathbf{x}) \leq -c_3 V(\mathbf{x})$$

hold for all $\mathbf{x} \in \mathcal{X}$ during the continuous phase of the K^{th} step, $\forall K \in \mathbb{Z}^+$ [21]. Then, one has $V|_K^- \leq e^{-c_3(T_{K+1}-T_K)} V|_{K-1}^+$.

Before analyzing the convergence of $\{V|_1^+, V|_2^+, V|_3^+ ...\}$, we first analyze the reset map in Eq. (16). From Eq. (16), one has

$$\begin{aligned} \|\mathbf{x}|_K^+\| =& \|\Delta(T_K^-, \mathbf{x}_f|_K^-)\| \\ \leq& \|\Delta(T_K^-, \mathbf{x}|_K^-) - \Delta(\tau_K^-, \mathbf{x}|_K^-)\| \\ &+ \|\Delta(\tau_K^-, \mathbf{x}|_K^-) - \Delta(\tau_K^-, \mathbf{0})\| \\ &+ \|\Delta(\tau_K^-, \mathbf{0})\|. \end{aligned} \tag{17}$$

Suppose that the desired trajectories $\mathbf{h}_d(t, \theta(\mathbf{q}))$ provided by a high-level planner is continuously differentiable in t. Then, the reset map Δ is continuously differentiable in t. It can also be proved that Δ is continuously differentiable in $\mathbf{x}$. Thus, there exists a positive number r_1 and Lipschitz constants L_{Δ_t} and L_{Δ_x} such that [15]

$$\|\Delta(T_K^-, \mathbf{x}|_K^-) - \Delta(\tau_K^-, \mathbf{x}|_K^-)\| \leq L_{\Delta_t}\|T_k - \tau_k\| \tag{18}$$

and

$$\|\Delta(\tau_K^-, \mathbf{x}|_K^-) - \Delta(\tau_K^-, \mathbf{0})\| \leq L_{\Delta_x}\|\mathbf{x}|_K^-\| \tag{19}$$

hold for any $\mathbf{x}(T_0) \in B_{r_1}(\mathbf{0})$.

Based on our previous study [15], it can be proved that there exists a positive number r_2 and a Lipschitz constant L_{T_x} such that

$$|T_K - \tau_K| \leq L_{T_x}\|\tilde{\mathbf{x}}(\tau_K; T_{K-1}^+, \mathbf{x}|_{K-1}^+)\| \tag{20}$$

for any $\mathbf{x}(T_0) \in B_{r_2}(\mathbf{0})$. Here, $\tilde{\mathbf{x}}(t; t_0, \lambda_0)$ represents a solution of $\dot{\tilde{\mathbf{x}}} = \mathbf{A}\tilde{\mathbf{x}}$ with the initial condition $\tilde{\mathbf{x}}(t_0) = \lambda_0$, $\forall t > t_0$.

If the desired trajectories satisfy the impact invariance condition in Eq. (13), then $\|\Delta(\tau_K^-, \mathbf{0})\| = \mathbf{0}$ always holds, which will greatly simplify the stability analysis as follows.

Equations (17) - (20) indicate that there exists a positive number L_d such that

$$\|\mathbf{x}|_K^+\| \leq L_d(\|\tilde{\mathbf{x}}(\tau_K; T_{K-1}^+, \mathbf{x}|_{K-1}^-)\| + \|\mathbf{x}|_K^-\|), \tag{21}$$

where, from the above analysis, one has

$$\|\mathbf{x}|_K^-\| \leq \sqrt{\frac{c_2}{c_1}} e^{-\frac{c_3}{2c_2}(T_K - T_{K-1})} \|\mathbf{x}|_{K-1}^+\|,$$

and

$$\|\tilde{\mathbf{x}}(\tau_K; T_{K-1}^+, \mathbf{x}|_{K-1}^-)\| \leq \sqrt{\frac{c_2}{c_1}} e^{-\frac{c_3}{2c_2}(\tau_k - T_{K-1})} \|\mathbf{x}|_{K-1}^+\|.$$

Hence, the equations above yield

$$\|\mathbf{x}|_K^+\| \leq L_d \sqrt{\tfrac{c_2}{c_1}} e^{-\frac{c_3}{2c_2}(\tau_K - T_{K-1})} (1 + e^{-\frac{c_3}{2c_2}(T_K - \tau_K)}) \|\mathbf{x}|_{K-1}^+\|. \tag{22}$$

Equation (22) shows that the convergence rate of the sequence $\{\mathbf{x}|_1^+, \mathbf{x}|_2^+, ...\}$ is $\frac{c_3}{2c_2}$, which is determined by the control gains in Eq. (16). Hence, $\{V|_1^+, V|_2^+, V|_3^+ ...\}$ will be a strictly decreasing sequence if the control gains are chosen such that the convergence rate $\frac{c_3}{2c_2}$ is sufficiently large.

In summary, the closed-loop hybrid system is locally exponentially stable if the control gains in Eq. (16) are chosen such that the matrix $\mathbf{A}$ in Eq. (16) is Hurwitz and that the continuous-phase convergence rate is sufficiently high.

IV. SIMULATIONS

This section presents the MATLAB [23] and Webots [24] simulation results on a NAO bipedal humanoid robot to demonstrate the effectiveness of the proposed control strategy in realizing exponential global-position tracking as well as to provide preliminary insights into hardware implementation.

A. Trajectory Generation

In both simulations and experiments, the same desired trajectories $\mathbf{h}_d(t, \theta(\mathbf{q}))$ will be used for convenience of comparison. The desired walking path Γ_d and the desired position trajectory $x_d(t)$ along the path are assumed to be provided by a high-level task planner because they both define critical desired behaviors of a bipedal robot when performing high-level tasks. Without loss of generality, the desired straight-line path is chosen as the X_W-axis of the world coordinate frame, and the desired position trajectory along Γ_d is chosen as $x_d(t) = 0.04t - 0.01$ (m).

The desired Beziér polynomials $\boldsymbol{\phi}(\theta)$ are planned through optimization-based motion planning. The Beziér polynomials are chosen as 6^{th}-order (i.e., $M = 6$), and their coefficients $\boldsymbol{\alpha}_k$ $(k = 0, 1, ..., M)$ are optimized to satisfy the following constraints: a) Impact invariance conditions in Eq. (13); b) Joint position and velocity limits; c) Holonomic constraints in Eq. (3); d) Desired gait properties (e.g., step length and maximum swing-foot elevation).

B. MATLAB Simulations

In MATLAB simulations, the proposed time-dependent input-output linearizing control strategy in Eq. (15) is implemented using the hybrid dynamic model presented in Section II. The control gains are set as $\mathbf{K}_p = K_p \mathbf{I}_{m\times m}$ $(K_p = 484)$ and $\mathbf{K}_d = K_d \mathbf{I}_{m\times m}$ $(K_d = 44)$. This choice of control gains will guarantee the stability of the linearized continuous-phase dynamics in Eq. (16).

Figure 2 shows the global-position tracking results, which indicate that the simulated NAO robot exponentially converges to the desired global path Γ_d and the desired position

trajectory $x_d(t)$ along the path despite the large initial tracking error.

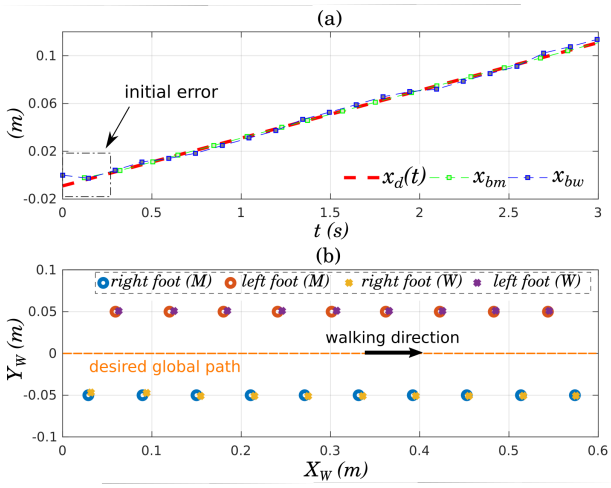

Fig. 2. Global-position tracking results in MATLAB and Webots simulations. The initial global-position tracking error is set as $x_{bm}(0) - x_d(0) = x_{bw}(0) - x_d(0) = -1$ cm, which is approximately $\frac{1}{3}$ of the step length. (a) Tracking results of $x_d(t)$. $x_{bm}(t)$ and $x_{bw}(t)$ are the actual global-position trajectories along Γ_d obtained in MATLAB and Webots simulations, respectively. Both of them demonstrate satisfactory tracking of the desired trajectory $x_d(t)$. (b) Tracking results of Γ_d. *left foot (M)* and *right foot (M)* are the actual support-foot placements in MATLAB simulations, and *left foot (W)* and *right foot (W)* are those in Webots simulations. Both of them indicate satisfactory tracking of the desired path Γ_d, which is the X_W-axis of the world coordinate frame.

C. Webots Simulations

Webots is a robot simulator that allows accurate simulation of dynamical, physical, and graphical properties of rigid-body objects. In this study, Webots simulations are conducted to help us gain preliminary insights into hardware implementation on the NAO robot.

The NAO robot has a major hardware limitation, that is, the robot does not allow users to send torque commands to joint actuators. Since the control input $\mathbf{u}$ in Eq. (15) is a torque signal, this limitation prevents the direct implementation of the proposed control law in Eq. (15).

To enable reliable global-position tracking for the NAO robot despite this hardware limitation, we adapt the proposed walking control strategy for the NAO robot and use Webots simulations to evaluate the adapted strategy on a robot model that emulates the NAO robot including its hardware limitation in actuator accessibility.

The proposed controller adaptation for the time step t is described as follows:

- At the time step t, the phase variable $\theta := x_b(t) - x_{st}$ is computed based on $x_b(t)$ and the current support-foot position along the X_W-axis, denoted as x_{st};
- The individual joint position $\mathbf{q}_d(t)$ is computed by solving $\mathbf{h}_c(\mathbf{q}_d(t)) - \mathbf{h}_d(t,\theta) = \mathbf{0}$;
- $\mathbf{q}_d$(t) is then fed into NAO's joint controller in Webots, which emulates the actual robot's default controller and drives the current configuration to the desired one.

To avoid drastic initial motion of the robot under large initial tracking errors, it has been found that θ can be replaced by $\theta_d := x_d(t) - x_{st}$ in the above algorithm until the robot converges sufficiently close to the desired trajectories.

Figure 2 shows the global-trajectory tracking performance in Webots simulations together with that in MATLAB simulations. One can notice that the green line (x_{bm}, MATLAB) exponentially converges to the desired trajectory $x_d(t)$ and that the blue line (x_{bw}, Webots) converges to a small neighborhood around $x_d(t)$. This discrepancy in tracking performance is primarily due to: a) The impact models in Webots and MATLAB are different; b) The implemented controllers are different. However, the satisfactory tracking results in Webots indicate the effectiveness of the proposed controller adaptation strategy in the presence of a NAO robot's hardware limitations.

V. EXPERIMENTS

In this section, we will present the experimental set-up, hardware implementation details, and the experimental results.

The experimental set-up for testing the global-position tracking performance of the proposed walking strategy is shown in Fig. 3. With this experimental set-up, the robot's general coordinates $\mathbf{q}$ in Eq. (1) can be readily obtained for controller implementation.

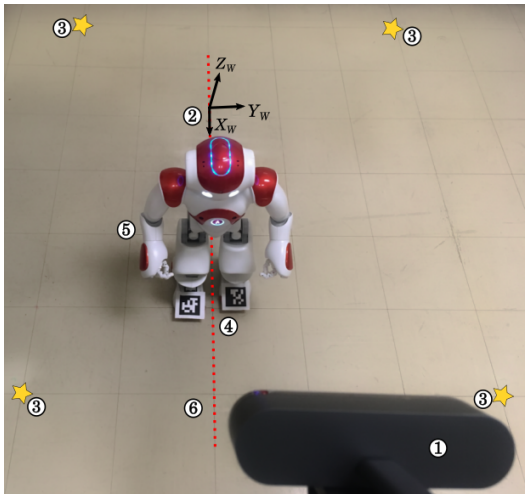

Fig. 3. Experimental set-up for testing the global-position tracking performance on the NAO bipedal robot. The labels refer to: (1) A Logitech 4K PRO WEBCAM. (2) The world coordinate frame. (3) The reference points for perspective transformation. (4) AprilTag attached on the NAO's feet, which is utilized to determine the robot's floating-base position, $\mathbf{p}_b$, in the world coordinate frame. (5) A NAO robot. (6) The desired global path.

Due to the NAO robot's limited actuator accessibility, it is necessary to adapt the proposed walking control strategy in Eq. (15) for hardware implementation. Since the control strategy adapted for Webots simulations can realize satisfactory global-position tracking on a robot model that emulates a NAO robot including its hardware limitation, it will be experimentally implemented.

Experimental results are illustrated in Fig. 4. It clearly shows that the proposed control strategy drives the robot's global position to reliably track both the desired position trajectory $x_d(t)$ and the desired global-path Γ_d.

Figures 2 and 4 also demonstrate that steady-state tracking accuracy is guaranteed even across rigid-body landing impacts in both simulations and experiments. This is because the impact invariance conditions are incorporated into motion planning such that the desired trajectory $\mathbf{h}_d$ respects the impact dynamics as explained in Section IV-A. Accordingly, the corresponding joint position $\mathbf{q}_d$, which is used as the desired joint position in Webots simulations and experiments, will also agree with the impact dynamics.

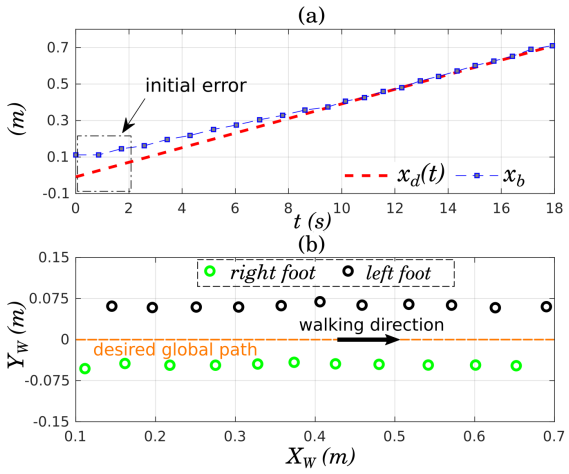

Fig. 4. Experimental results of global-position tracking with the proposed walking control Strategy. The initial global-position tracking error is set as $x_b(0) - x_d(0) = -1$ cm, which is approximately $\frac{1}{3}$ of the step length. (a) Results of tracking $x_d(t)$. As clearly shown in the plot, the proposed walking control strategy guarantees accurate tracking of the desired trajectory $x_d(t)$. (b) Results of tracking Γ_d. The results demonstrate that the proposed walking control strategy guarantees accurate tracking of the desired global path Γ_d.

VI. CONCLUSIONS

In this paper, we have theoretically synthesized a time-dependent global-position tracking controller for 3-D fully actuated bipedal robotic walking and experimentally validated it on a NAO bipedal humanoid robot. The proposed controller was theoretically established through full-order dynamic modeling, model-based state feedback control, and Lyapunov-based stability analysis, which can achieve reliable global-position tracking for enhancing walking versatility. Due to limited actuator accessibility of the NAO robot, necessary adaptation of the proposed walking controller was made for hardware implementation. Both simulation and experimental results validated the effectiveness of the proposed walking strategy. The results of this paper can be used to guide hardware implementation of global-position tracking control on legged robots with the common hardware limitation of actuator accessibility, thus helping to bridge the gap between theory and experiment.

REFERENCES

[1] D. G. E. Hobbelen and M. Wisse, "Limit cycle walking," in *Humanoid Robots, Human-like Machines*, 2007.

[2] M. Vukobratović and B. Borovac, "Zero-Moment Point: thirty five years of its life," *International Journal of Humanoid Robotics*, vol. 1, no. 01, pp. 157–173, 2004.

[3] S. Kajita, M. Morisawa, K. Miura, S. Nakaoka, K. Harada, K. Kaneko, F. Kanehiro, and K. Yokoi, "Biped walking stabilization based on linear inverted pendulum tracking," in *Proc. of IEEE/RSJ International Conference on Intelligent Robots and Systems*, pp. 4489–4496, 2010.

[4] M. J. Powell, A. Hereid, and A. D. Ames, "Speed regulation in 3D robotic walking through motion transitions between human-inspired partial hybrid zero dynamics," in *Proc. of IEEE International Conference on Robotics and Automation*, pp. 4803–4810, 2013.

[5] J. W. Grizzle, G. Abba, and F. Plestan, "Asymptotically stable walking for biped robots: Analysis via systems with impulse effects," *IEEE Transactions on Automatic Control*, vol. 46, no. 1, pp. 51–64, 2001.

[6] R. Tedrake, S. Kuindersma, R. Deits, and K. Miura, "A closed-form solution for real-time ZMP gait generation and feedback stabilization," in *Proc. of IEEE-RAS International Conference on Humanoid Robots*, pp. 936–940, 2015.

[7] E. R. Westervelt, J. W. Grizzle, and D. E. Koditschek, "Hybrid zero dynamics of planar biped walkers," *IEEE Transactions on Automatic Control*, vol. 48, no. 1, pp. 42–56, 2003.

[8] R. W. Sinnet, M. J. Powell, R. P. Shah, and A. D. Ames, "A human-inspired hybrid control approach to bipedal robotic walking," *Proc. of IFAC*, vol. 44, no. 1, pp. 6904–6911, 2011.

[9] A. Hereid, E. A. Cousineau, C. M. Hubicki, and A. D. Ames, "3D dynamic walking with underactuated humanoid robots: A direct collocation framework for optimizing hybrid zero dynamics," in *Proc. of IEEE International Conference on Robotics and Automation*, pp. 1447–1454, 2016.

[10] M. J. Powell, W.-L. Ma, E. R. Ambrose, and A. D. Ames, "Mechanics-based design of underactuated robotic walking gaits: Initial experimental realization," in *Proc. of IEEE-RAS International Conference on Humanoid Robots*, pp. 981–986, 2016.

[11] A. Hereid, S. Kolathaya, M. S. Jones, J. Van Why, J. W. Hurst, and A. D. Ames, "Dynamic multi-domain bipedal walking with ATRIAS through SLIP based human-inspired control," in *Proc. of ACM International Conference on Hybrid Systems: Computation and Control*, pp. 263–272, 2014.

[12] K. Sreenath, H.-W. Park, I. Poulakakis, and J. W. Grizzle, "Embedding active force control within the compliant hybrid zero dynamics to achieve stable, fast running on MABEL," *The International Journal of Robotics Research*, vol. 32, no. 3, pp. 324–345, 2013.

[13] A. E. Martin and R. D. Gregg, "Stable, robust hybrid zero dynamics control of powered lower-limb prostheses," *IEEE Transactions on Automatic Control*, vol. 62, no. 8, pp. 3930–3942, 2017.

[14] X. Da, R. Hartley, and J. W. Grizzle, "Supervised learning for stabilizing underactuated bipedal robot locomotion, with outdoor experiments on the wave field," in *Proc. of IEEE International Conference on Robotics and Automation*, pp. 3476–3483, 2017.

[15] Y. Gu, B. Yao, and C. G. Lee, "Bipedal gait recharacterization and walking encoding generalization for stable dynamic walking," in *Proc. of IEEE International Conference on Robotics and Automation*, pp. 1788–1793, 2016.

[16] Y. Gu, B. Yao, and C. G. Lee, "Exponential stabilization of fully actuated planar bipedal robotic walking with global position tracking capabilities," *Journal of Dynamic Systems, Measurement, and Control*, vol. 140, no. 5, p. 051008, 2018.

[17] Y. Gu, B. Yao, and C. G. Lee, "Straight-line contouring control of fully actuated 3-D bipedal robotic walking," in *Proc. of American Control Conference*, pp. 2108–2113, 2018.

[18] "Softbank robotics." http://www.robotis.us/robotis-OP2-OP3/. Accessed: 2018-09-20.

[19] D. Kim, J. Lee, O. Campbell, H. Hwang, and L. Sentis, "Computationally-robust and efficient prioritized whole-body controller with contact constraints," *arXiv preprint arXiv:1807.01222*, 2018.

[20] E. R. Westervelt, C. Chevallereau, J. H. Choi, B. Morris, and J. W. Grizzle, *Feedback control of dynamic bipedal robot locomotion*. CRC press, 2007.

[21] H. K. Khalil, *Noninear systems*. No. 5, Prentice Hall, 1996.

[22] M. S. Branicky, "Multiple lyapunov functions and other analysis tools for switched and hybrid systems," *IEEE Transactions on Automatic Control*, vol. 43, no. 4, pp. 475–482, 1998.

[23] "The MathWorks, Inc." https://www.mathworks.com/. Accessed: 2018-09-20.

[24] "Cyberbotics ltd." https://cyberbotics.com/. Accessed: 2018-09-20.